Geoscience Frontiers 10 (2019) 1125–1138

HOSTED BY

Contents lists available at ScienceDirect

China University of Geosciences (Beijing)

Geoscience Frontiers

journal homepage: www.elsevier.com/locate/gsf

Research Paper

The role of aluminium in the preservation of microbial biosignatures

Alan Levett [a,*], Emma J. Gagen [a], Hui Diao [b], Paul Guagliardo [c], Llew Rintoul [d], Anat Paz [a], Paulo M. Vasconcelos [a], Gordon Southam [a]

[a] School of Earth and Environmental Sciences, University of Queensland, Brisbane, Queensland 4072, Australia
[b] Centre for Microscopy and Microanalysis, University of Queensland, Brisbane, Queensland 4072, Australia
[c] Centre for Microscopy, Characterisation and Analysis, University of Western Australia, Perth 6009, Western Australia, Australia
[d] School of Chemistry, Physics & Mechanical Engineering, Queensland University of Technology, Brisbane, Queensland 4001, Australia

ARTICLE INFO

Article history:
Received 1 December 2017
Received in revised form
23 April 2018
Accepted 10 June 2018
Available online 27 July 2018
Handling Editor: Stijn Glorie

Keywords:
Aluminium
Microfossils
Biosignatures
NanoSIMS
Organomineralisation

ABSTRACT

Demonstrating the biogenicity of presumptive microfossils in the geological record often requires supporting chemical signatures, including isotopic signatures. Understanding the mechanisms that promote the preservation of microbial biosignatures associated with microfossils is fundamental to unravelling the palaeomicrobiological history of the material. Organomineralization of microorganisms is likely to represent the first stages of microbial fossilisation and has been hypothesised to prevent the autolytic degradation of microbial cell envelope structures. In the present study, two distinct fossilisation textures (permineralised microfossils and iron oxide encrusted cell envelopes) identified throughout iron-rich rock samples were analysed using nanoscale secondary ion mass spectrometry (NanoSIMS). In this system, aluminium is enriched around the permineralised microfossils, while iron is enriched within the intracellularly, within distinct cell envelopes. Remarkably, while cell wall structures are indicated, carbon and nitrogen biosignatures are not preserved with permineralised microfossils. Therefore, the enrichment of aluminium, delineating these microfossils appears to have been critical to their structural preservation in this iron-rich environment. In contrast, NanoSIMS analysis of mineral encrusted cell envelopes reveals that preserved carbon and nitrogen biosignatures are associated with the cell envelope structures of these microfossils. Interestingly, iron is depleted in regions where carbon and nitrogen are preserved. In contrast aluminium appears to be slightly enriched in regions associated with remnant cell envelope structures. The correlation of aluminium with carbon and nitrogen biosignatures suggests the complexation of aluminium with preserved cell envelope structures before or immediately after cell death may have inactivated autolytic activity preventing the rapid breakdown of these organic, macromolecular structures. Combined, these results highlight that aluminium may play an important role in the preservation of microorganisms within the rock record.

1. Introduction

Microbial fossils provide insights into the environmental conditions in which they existed, revealing information about how microorganisms interacted with their environments. Microorganisms may be fossilised in diverse environmental conditions and preserved by interactions with various elements and minerals. Silicification (Konhauser et al., 2004), calcification (Riding, 2000) and ferrugination in acidic (Preston et al., 2011) and neutral environments (Salama et al., 2013) may be responsible for the preservation of bacteriomorphic structures. Within iron-rich environments, electrostatic interactions between iron cations and net negative cell envelopes have been proposed to drive the biomineralization of microorganisms, which has been postulated to represent the first stage of microbial fossilisation (Ferris et al., 1988; Li et al., 2013, 2014). The present study aimed to determine the chemical biosignatures associated with fossilised microorganisms in near-neutral iron-rich environments.

* Corresponding author.
E-mail address: alan.levett@uqconnect.edu.au (A. Levett).
Peer-review under responsibility of China University of Geosciences (Beijing).

https://doi.org/10.1016/j.gsf.2018.06.006

Aluminium is the third most abundant element within the Earth's crust, with only oxygen and silicon more abundant. Despite the plenitude of aluminium, it serves no known biological function and is generally toxic in labile forms to most microorganisms (Exley and Birchall, 1992). Aluminium mobility is primarily controlled by pH, although the solubility of minerals containing aluminium and organic acids also influence the release and subsequent stability of aluminium ions in solution (Bache, 1986). Below pH 5, the prominent ionic aluminium species is $Al(H_2O)_6^{3+}$, typically referred to as Al^{3+} or free aluminium, which is considered to be the most inimical to biota (Macdonald and Martin, 1988). Insoluble $Al(OH)_3$ precipitates reach a maximum at pH of approximately 6.2, which coincides with the minimum solubility of free aluminium (Martin, 1986). At circumneutral pH, aluminium is relatively immobile and generally considered nontoxic (Bache, 1986). In alkaline solutions ($pH \geq 7.4$), $Al(OH)_3$ precipitates begin to redissolve, forming $Al(OH)_4^-$ complexes (Macdonald and Martin, 1988).

Aluminium binding to cell envelope structures of *Escherichia coli* (Guida et al., 1991) has been demonstrated; however, the role of aluminium in microbial fossilisation and the preservation of organic biosignatures has not previously been reported.

Determining the biogenicity of bacteriomorphic structures within the geologic record based can be misleading (Marshall et al., 2011). Chemical or isotopic signatures to support the preservation of microbial fossils are often required to ascertain the biological origins of microfossils (Brasier et al., 2015). Here, two distinct microbial fossilisation textures identified in iron-rich environments using scanning electron microscopy were examined using nanoscale secondary ion mass spectrometry (NanoSIMS), revealing a role for aluminium in the preservation of structural ± organic biosignatures.

2. Materials and methods

2.1. Site description and sample collection

2.1.1. Carajás sample-ferruginous duricrust

A ferruginous duricrust hand-sample was collected from eastern aspect of the Carajás mineral province in the State of Pará, Brazil (Vale S.A. N1 site). The hand-sample collected was of a well consolidated ferruginous duricrust that caps highly weathered banded iron formation (BIF). The duricrust sample was collected in proximity to a large lake and was likely to have been previously submerged during the summer months (November–March) when the Carajás mineral province receives the bulk of its annual rainfall (approximately 1800 mm). The ferruginous duricrust sample from the lake-edge was extremely competent, hard and appeared to be less porous than ferruginous duricrust that formed away from the lake-edge. Ferruginous duricrusts in the Carajás typically cap the weathering profile of BIFs and are associated with little to no soil profile. The sample was collected directly from the surface using a rock hammer in the complete absence of any soil. Consistent with the general description of ferruginous duricrusts that cap BIFs by Dorr (1964), the sample contains detrital fragments of high-grade specular hematite cemented by secondary bands of vitreous and dull goethite. Secondary goethite bands that indicate the flow of iron-rich solutions made this sample of interest to investigate the presence of microbial fossils and their role in the evolution of ferruginous duricrusts (Levett et al., 2016).

2.1.2. Quadrilátero Ferrífero sample – goethite-cemented vein

A hand sample from an exposed goethite-cemented vein was collected from the saprolite (~15 m in depth) of a highly

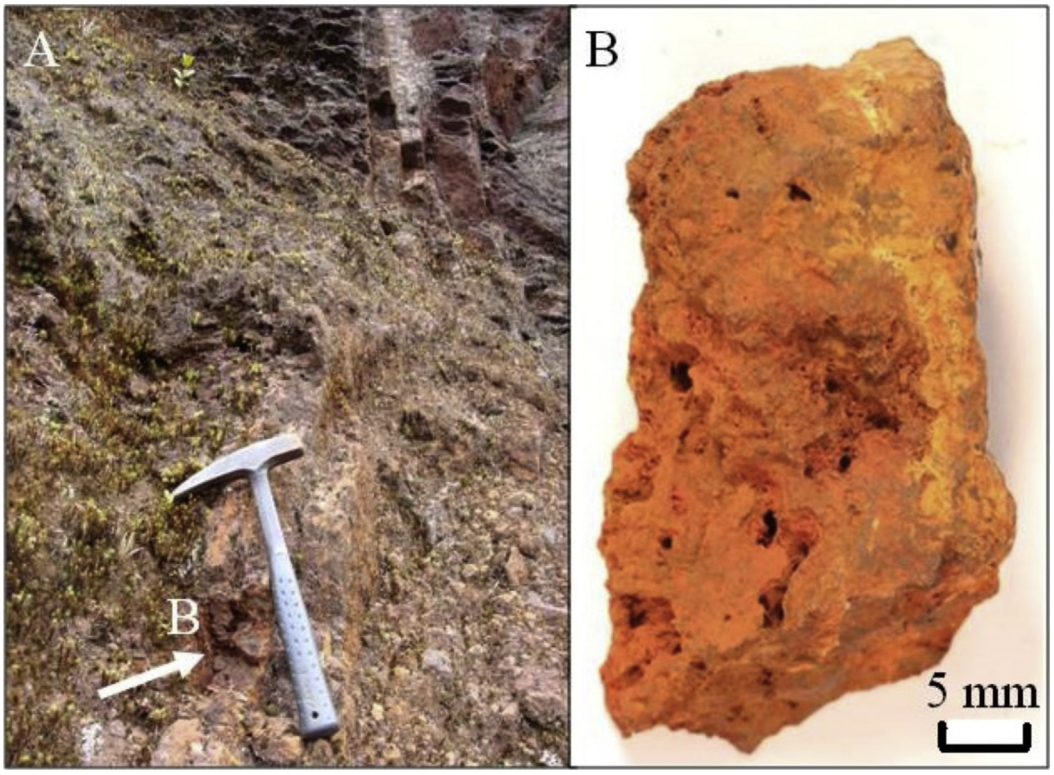

Figure 1. (A) Photograph of goethite cemented vein in the exposed saprolite from Serra do Gandarela, Quadrilátero Ferrífero (QF), State of Minas Gerais, Brazil. The white arrow indicates the region from which the hand sample was collected, approximately 15 m below the surface. (B) Photograph of goethite-cemented hand sample highlighting the presence of iron oxide coated roots.

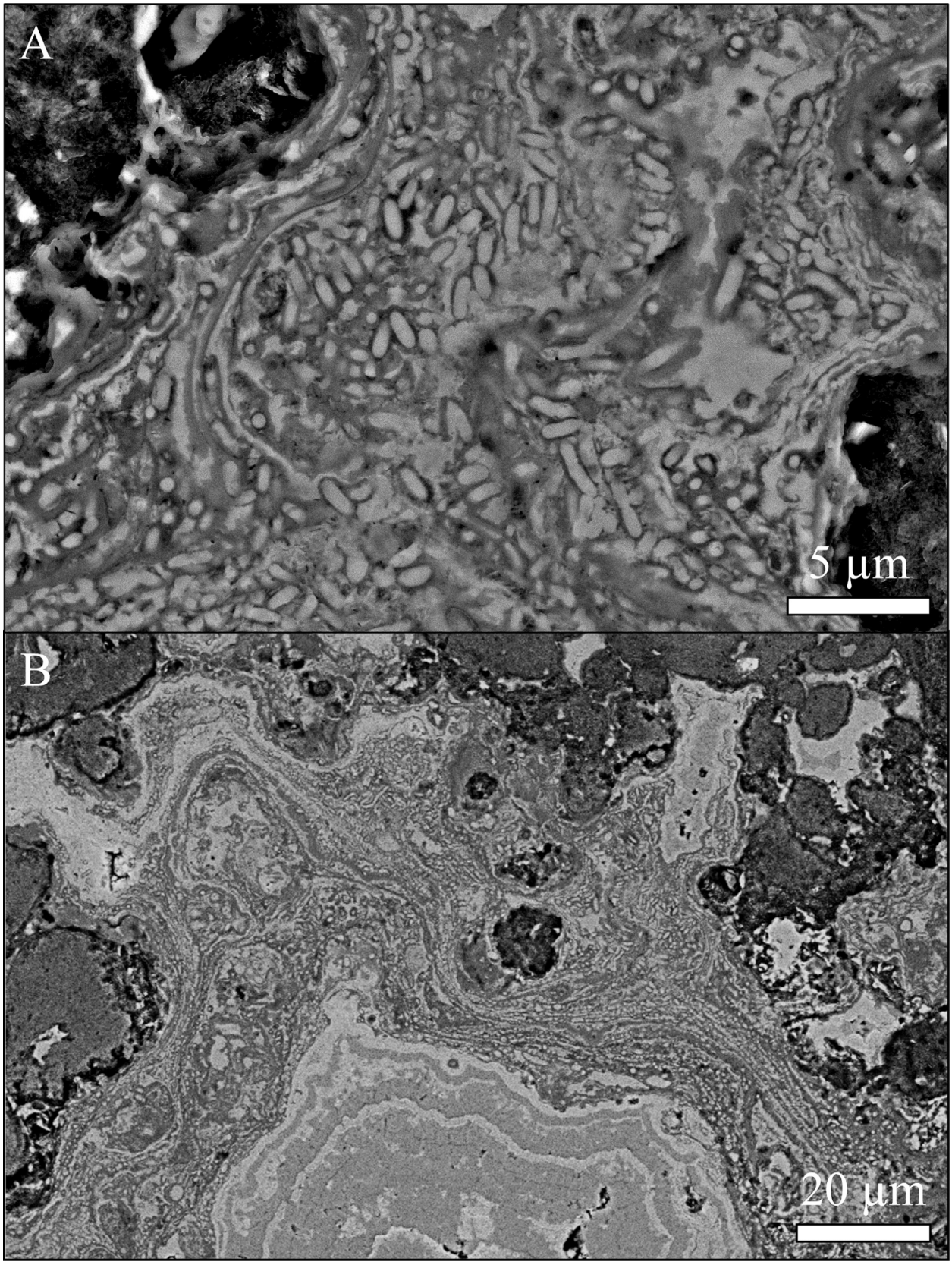

Figure 2. Backscattered scanning electron Field Emission micrographs highlighting rod-shaped microfossils (A) and large permineralised microbial biofilms (B) within an iron-rich duricrust capping iron ore deposits in the Carajás mineral province, State of Pará, Brazil. Permineralised microfossils formed around highly weathered kaolinite-rich clasts.

weathered banded iron formation profile from Serra do Gandarela, Quadrilátero Ferrífero in the State of Minas Gerais, Brazil (Fig. 1). The Quadrilátero Ferrífero (QF) has a tropical sub-humid climate with an approximate annual rainfall of 1900 mm during the summer months (November–March). Temperatures in the QF are typically between 13 °C and 30 °C year round with temperatures of up to 70 °C recorded over bare rocks (Jacobi and Carmo, 2011). The geology and geochemistry of the QF have been previously presented (Spier et al., 2003). The goethite-cemented vein was closely associated with the roots of small shrubs, which had become coated in iron oxide precipitates (Fig. 1A). The sample contains well consolidated goethite and hematite with dull secondary goethite precipitates within pore spaces and covering grain surfaces (Fig. 1B).

2.2. Sample characterisation

Bulk sample pH, elemental composition and mineralogy of samples (see Fig. 1) from the Carajás mineral province (permineralised microfossils) and the Quadrilátero Ferrífero (encrusted cell envelopes) were determined to characterise the samples. For all analyses, rock samples were crushed to less than 62 μm using a ring and puck mill. The bulk sample pH was determined by mixing 1 g of sample with 5 mL of ultrapure water, agitating for 2 h and measuring the pH of the solution.

Bulk sample chemical compositions were determined using X-ray fluorescence (XRF) spectroscopy at the Australian Laboratory Services (Analytical Geochemistry). Samples were fused with a lithium tetraborate:lithium metaborate flux (including lithium nitrate as an oxidising agent) with a ratio of 12:22. Fused samples were poured into a platinum mould and analysed using XRF spectroscopy. Loss on ignition was calculated at 1000 °C.

Fourier transform infrared spectroscopy (FTIR) was used to identify the mineralogy of the grains associated with the permineralised microfossils and the encrusted cell envelopes. Briefly, a Nicolet iS50 FTIR spectrometer coupled with a continuum infrared microscope equipped with a Mercury-Cadmium-Telluride detector was operated in attenuated total reflection (micro-ATR) mode using a germanium crystal. Samples were analysed for 64 scans using an effective 40 μm × 40 μm spot size. Spectra were collected in the mid-infrared spectrum (4000–650 cm^{-1}) with a spectral resolution of 4 cm^{-1}.

2.3. Electron microscopy

Polished petrographic thin sections were made from rock samples from the Quadrilátero Ferrífero and the Carajás mineral province to characterise the microstructure of each rock sample. The microstructure of both samples was analysed to determine the role of microorganisms in the biogeochemical cycling of iron within highly weathered BIFs (Levett et al., 2016). A BAL-TEC MSC-010 sputter coater was used to coat petrographic thin sections with 10 nm iridium. A JEOL JSM-7100F Field Emission scanning electron microscope (FE-SEM) equipped with an energy dispersive X-ray spectrometer (EDS) was used to examine polished petrographic thin sections. High resolution SEM micrographs were acquired using accelerating voltages of 3–15 kV, with low voltages used for discerning surface features in secondary electron mode. Sample surfaces were cleaned using a XEI Scientific Evactron 25 Decontaminator RF Plasma Cleaning System and samples were degassed at 50 °C for a minimum of 12 h prior to examination.

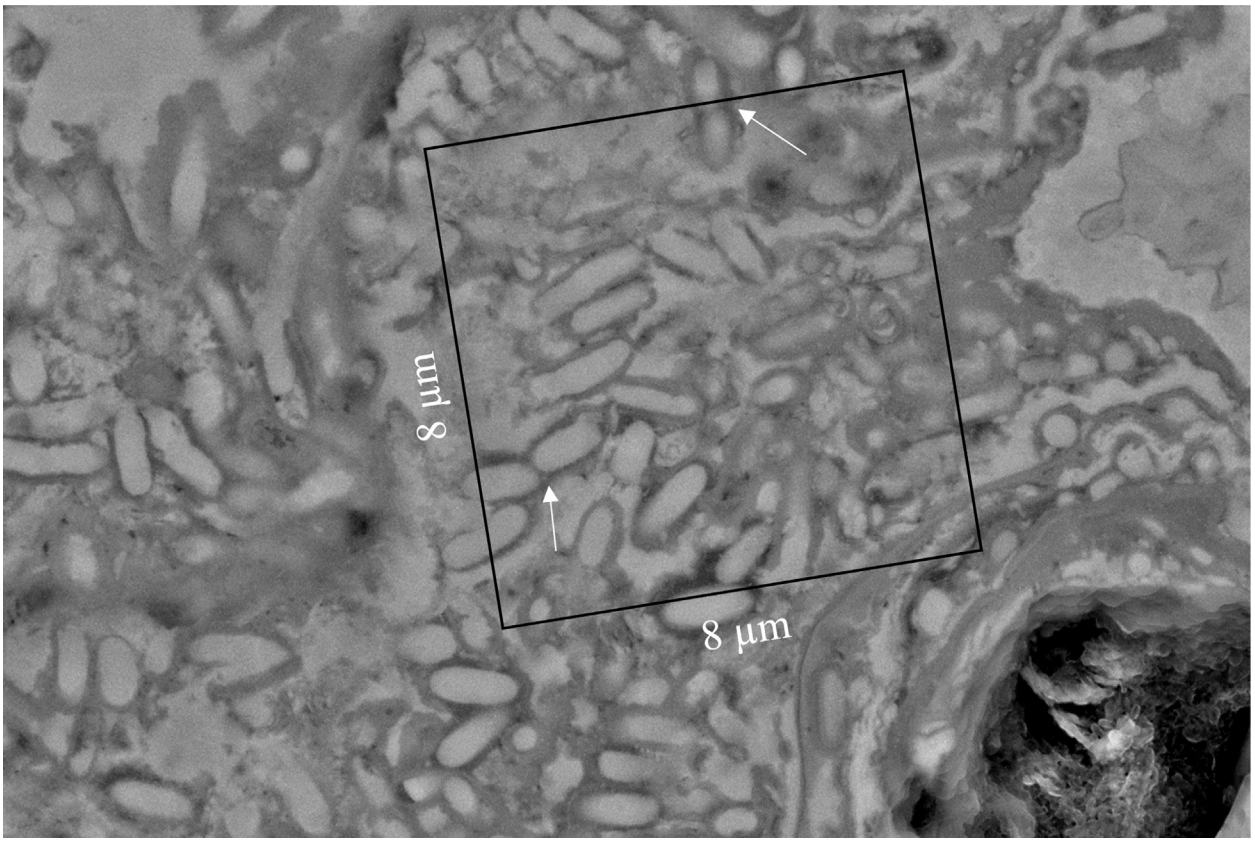

Figure 3. High resolution backscattered electron micrograph of rod-shaped permineralised microfossils, with evidence of colony formation and cell replication (arrows). The rectangle highlights the region analysed using NanoSIMS (refer to Fig. 4).

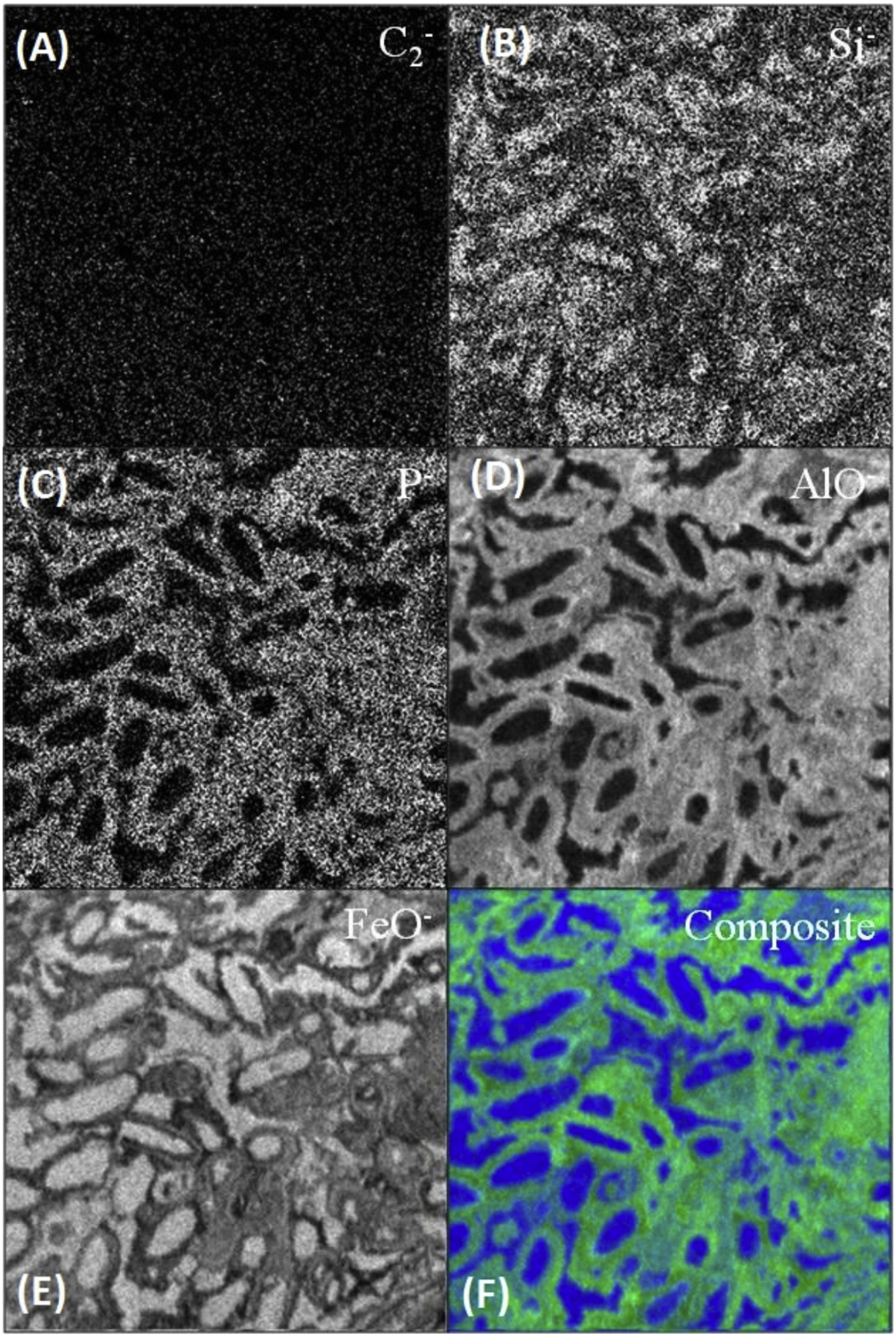

Figure 4. (A, B) NanoSIMS micrographs of permineralised microfossils presented as black and white intensity maps, with white areas having a higher relative elemental concentration compared with darker regions. NanoSIMS micrographs reveal that organic biosignatures are not preserved with permineralzsed microfossils. (C) Phosphorus colocalises with aluminium ($r = 0.41$). (D) Aluminium is enriched around the microfossils, while (E) iron is enriched within the intracellular regions of microfossils. (F) The composite micrograph highlights aluminium (green) enrichment around microfossils, with iron (blue) enriched within intracellular regions. All micrographs are 8 μm × 8 μm.

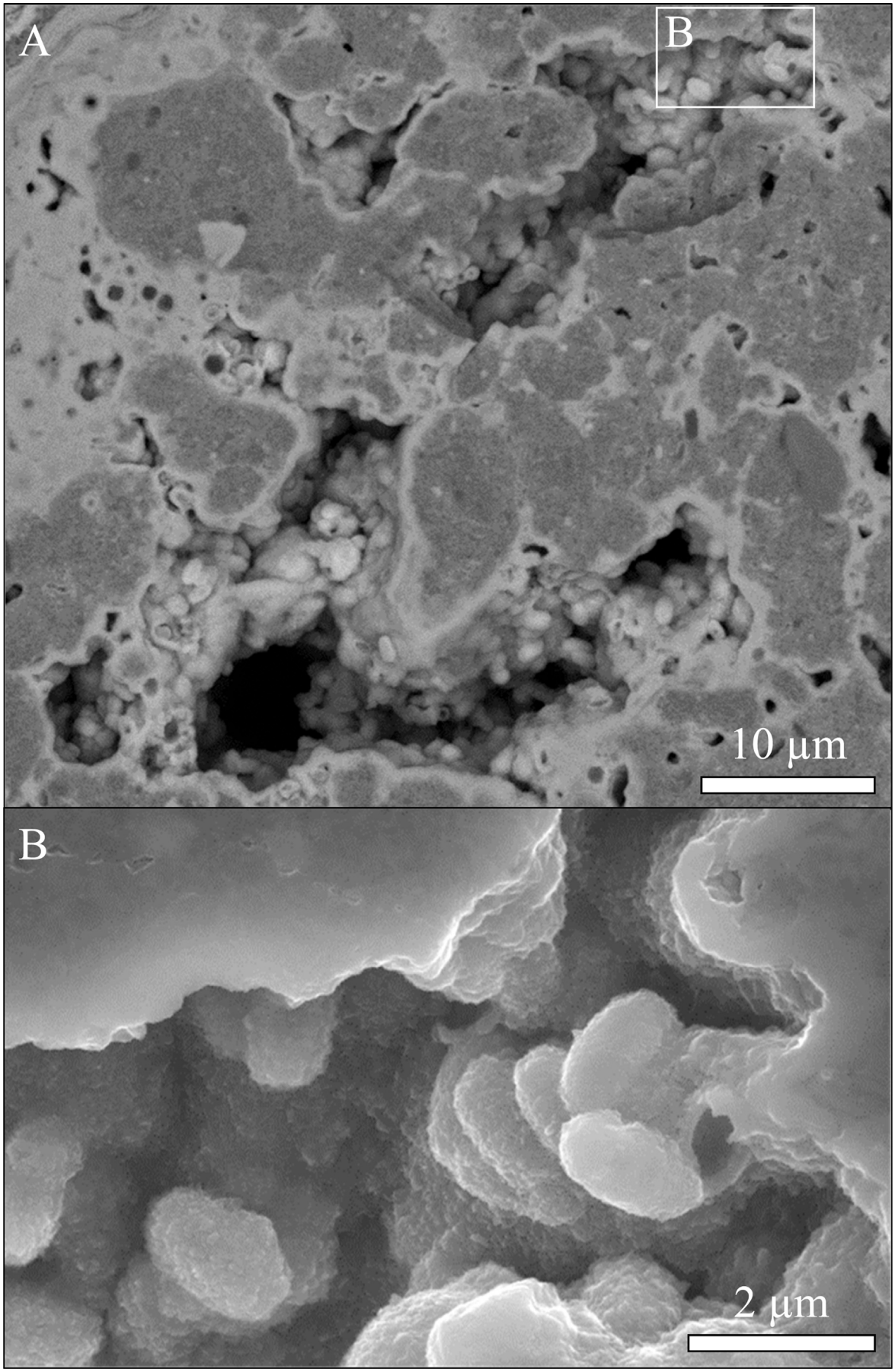
A
B
10 μm
B
2 μm

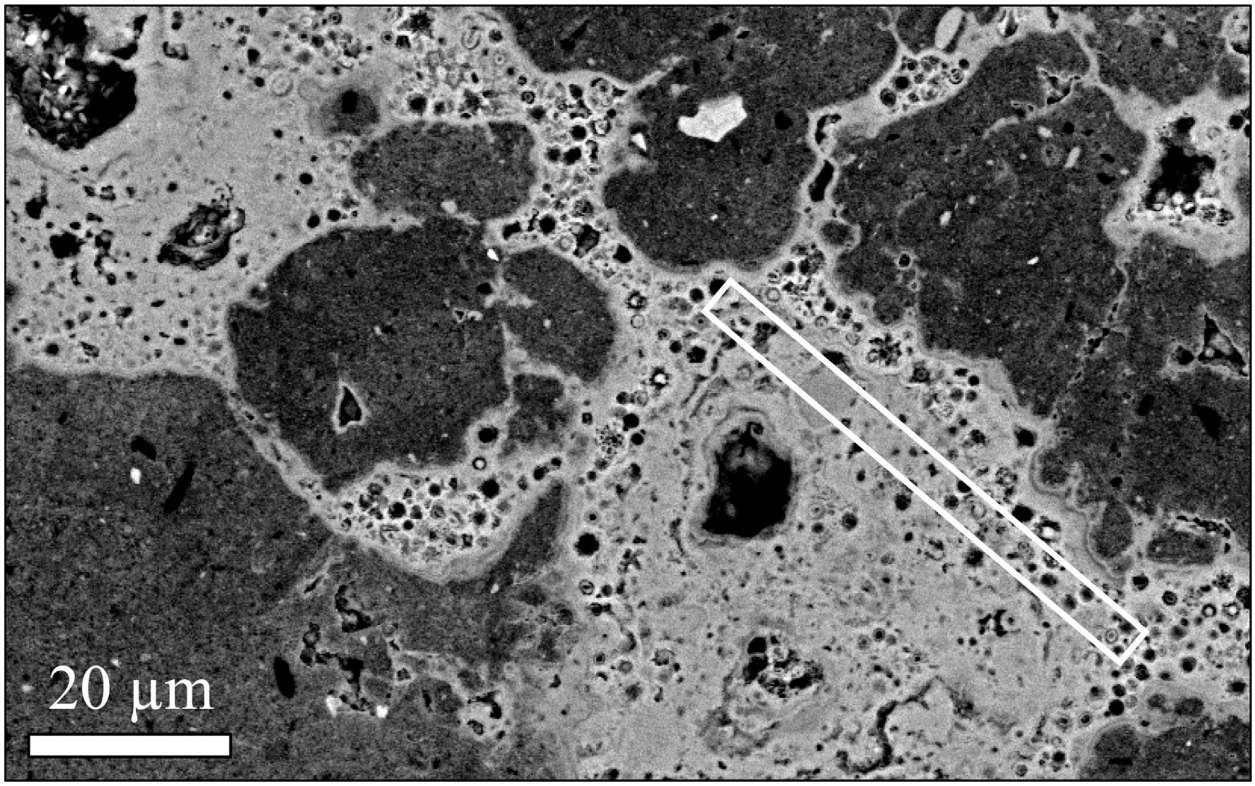

Figure 6. Backscattered scanning electron micrograph of encrusted cell envelopes that had infilled pore spaces between gibbsite-rich clasts. The rectangle highlights the regions from which a lamella was extracted using a focused ion beam scanning electron microscope for NanoSIMS analysis (refer to Figs. 7 and 8).

2.4. Nanoscale secondary ion mass spectrometry

2.4.1. Sample preparation

Permineralised microfossils were polished following the methods described by Levett et al. (2016). Briefly, ferruginous duricrust samples were hand polished using new, fixed SiC adhesives before a submicron diamond polish. Samples were adhered to a 1-inch diameter probe mount using Araldite (HY951). Samples were not embedded in an epoxy resin. All samples were coated with 5–10 nm gold prior to NanoSIMS analysis. Regions possessing microfossils (Fig. 2) were identified using BSE-SEM and targeted at high resolution (Fig. 3) for NanoSIMS (Fig. 4).

Encrusted microbial cell envelopes (Fig. 5) identified using BSE-SEM were prepared for nanoscale secondary ion mass spectrometry (NanoSIMS) using a FEI SCIOUS Focused Ion Beam – Scanning Electron Microscope (FIB-SEM) DualBeam system with lift-out capabilities. A large lamella (approximately 40 µm × 60 µm and 5 µm in depth) was extracted from polished petrographic thin sections using an up-scaled transmission electron microscope lamella preparation technique (Heaney et al., 2001). Briefly, large trenches were milled on both sides of the area of interest (Fig. 6), followed by a U-cut using a 50 nA gallium probe at an accelerating voltage of 30 kV. The lamella was extracted vertically using the EasyLift Manipulator system, allowing a previously unexposed cross-sectional area to be analysed using NanoSIMS. Sample preparation using the FIB-SEM preserved the structure of the encrusted cell envelopes (Fig. 7) and allowed for sample preparation away from resin, reducing potential sample contamination. The lamella was attached to a copper half grid using ion beam induced platinum deposition. The lamella was polished using decreasing beam currents to remove sample surface striations. A final step of low energy FIB polishing was carried out at 3 nA to reduce the ion beam damage on the sample's surface.

2.4.2. NanoSIMS analysis

Elemental maps were acquired for encrusted microbial cell envelopes and permineralised microfossils using the CAMECA NanoSIMS 50 (CAMECA, Paris, France) at the University of Western Australia, which allows for the simultaneous collection of 5 ions. In this experiment, to maximise the spatial resolution of the NanoSIMS, elemental maps were acquired using the Cs^+ ion beam, which was focused to a diameter of approximately 50 nm with a beam current of 0.3 pA. The primary Cs^+ beam was used to sputter secondary ions to investigate biosignatures preserved within an iron-rich matrix. For permineralised microfossils $^{12}C_2^-$, $^{28}Si^-$, $^{31}P^-$, $^{27}Al^{16}O^-$, $^{56}Fe^{16}O^-$ secondary ions were collected. Preliminary maps of permineralised microfossils revealed that CN^- cluster ions were not preserved, therefore only C_2^- ions were measured in high-resolution maps. For encrusted cell envelopes, $^{12}C_2^-$, $^{12}C^{14}N^-$, $^{31}P^-$, $^{27}Al^{16}O^-$, $^{56}Fe^{16}O^-$ secondary ions where collected. It should be noted that nitrogen cannot be measured directly using NanoSIMS, therefore the carbon-nitrogen cluster ion was measured to determine the presence of

Figure 5. Field Emission scanning electron micrographs of mineral encrusted cell envelope structures identified within a goethite cemented vein that cross-cut the saprolite of a weathered banded iron formation in the Serra do Gandarela, Quadrilátero Ferrífero in the State of Minas Gerais, Brazil. (A) Backscattered electron micrograph highlighting the preservation of encrusted cell envelopes within pore spaces. (B) Secondary electron micrograph of encrusted cell envelopes highlighting the three-dimensional preservation of encrusted cell envelopes that had formed in pore spaces.

nitrogen biosignatures associated with microfossils. Aluminium-oxide and iron-oxide cluster ions were measured to allow iron and aluminium to be mapped with carbon, nitrogen and phosphorus simultaneously, collecting secondary ions from a single plane. High resolution elemental micrographs were acquired by rastering the beam over a field of view of 8 μm × 8 μm at a resolution of 256 pixel × 256 pixel with a dwell time of 40–50 ms per pixel. Samples were pre-sputtered using the Cs^+ ion beam to remove any surface contamination and implant Cs^+ into the sample surfaces.

FIJI software was used to produce NanoSIMS chemical micrographs of permineralised microfossils and encrusted cell envelopes. Semi-quantitative NanoSIMS maps are presented as black and white intensity maps, with white areas having a higher relative elemental concentration compared with darker regions (Hoppe et al., 2013).

For permineralised microfossils, the colocalisation between phosphorus and aluminium for the permineralised microfossils was determined based on the Pearson correlation coefficient (r) for the entire region analysed using NanoSIMS.

For encrusted cell envelopes, cross-sections of individual microfossils ($n = 2$) were analysed to determine the correlation of preserved carbon and nitrogen with aluminium and iron. To achieve this, cross-sections of individual cells were plotted as pixel distance against ion counts. The Pearson correlation coefficient (r) was calculated to determine the correlation between carbon and nitrogen with iron and aluminium.

3. Results

Field Emission scanning electron microscopy was used to reveal two distinct microfossil textures preserved within iron-rich environments: permineralised microfossils (Figs. 2–4) and cell envelope structures encrusted in iron oxide minerals (Figs. 5–8). Nanoscale secondary ion spectrometry (NanoSIMS) highlighted that aluminium is enriched around permineralised microfossils, which appears to govern the structural preservation of permineralised microfossils (Fig. 4). For encrusted cell envelopes, NanoSIMS reveals that aluminium is enhanced in regions with preserved carbon and nitrogen biosignatures, which are likely to be remnant organic cell envelope structures (Fig. 8). The correlation of aluminium with organic carbon and nitrogen is highlighted by intensity cross-sections of individual cells (regions of interest; ROI) where ion counts are plotted against pixel distance (Fig. 9). Iron concentrations are depleted in all regions where carbon and nitrogen are preserved (Fig. 9). The carbon and nitrogen biosignatures associated with the encrusted cell envelopes are referred to as organic biosignatures.

3.1. Permineralised microfossils

The lake-edge ferruginous duricrust sample in which the permineralised microfossils are identified has an approximate pH of 6.5. X-ray diffraction data indicate that goethite and hematite are the dominant minerals present in the duricrust sample with minor kaolinite (Supplementary Fig. A1). The duricrust sample is primarily composed of Fe (52.64 wt.%), Al_2O_3 (8.63 wt.%) and SiO_2 (4.92 wt.%), with minor TiO_2 (0.85 wt.%) and P (0.227 wt.%). All other cations are below 0.1% (Table 1). Microfossil morphologies are typically rod-shaped, ranging of 0.5–1 μm in diameter and 1.5–2 μm in length (Fig. 3). Evidence of cell-replication (Fig. 3; arrows) and colony formation highlight these structures represent fossilised microorganisms. Relatively large microbial clusters

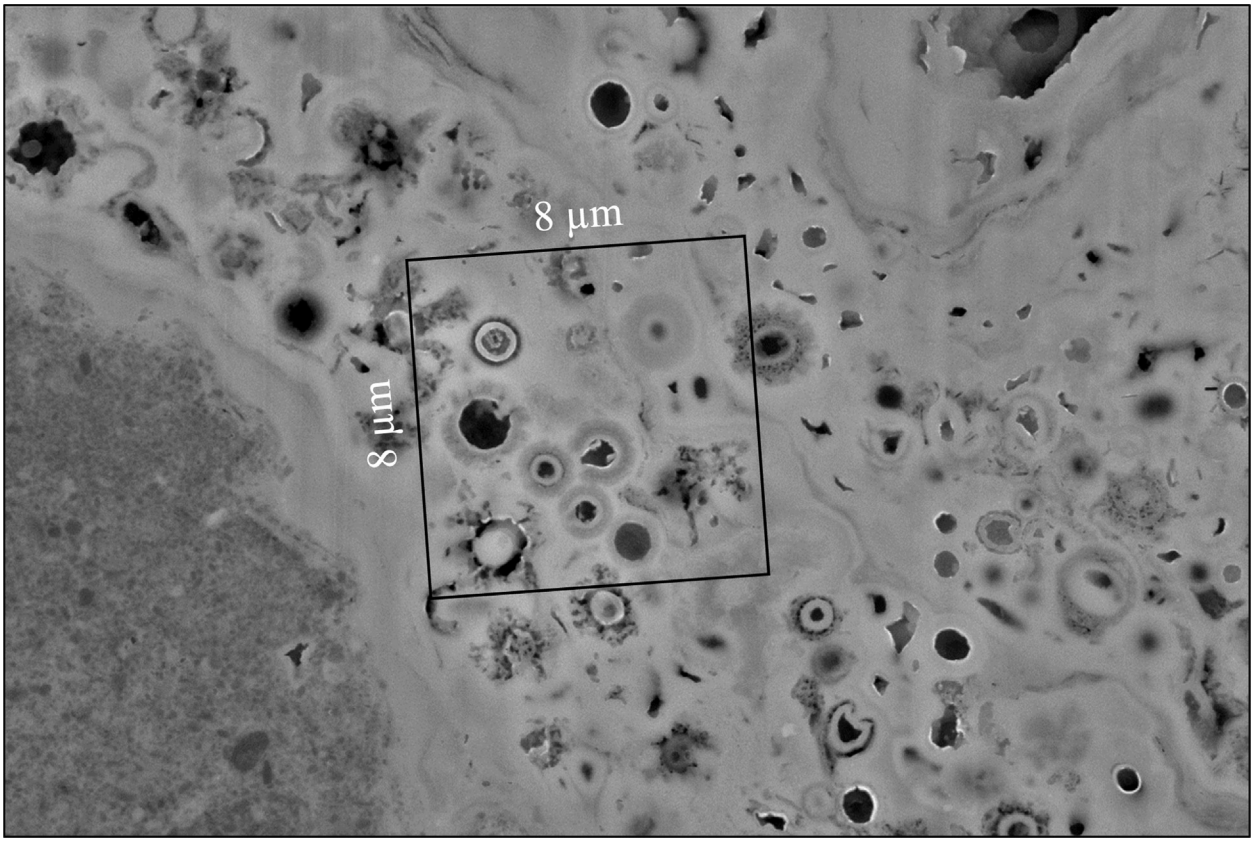

Figure 7. High resolution backscattered electron Field Emission micrograph of encrusted cell envelope sample that had been extracted using a focused ion beam scanning electron microscope from the region highlighted in Fig. 2. A variety of fossilisation textures were associated with the encrusted cell envelopes. The rectangle represents the region analysed using NanoSIMS (refer to Fig. 8).

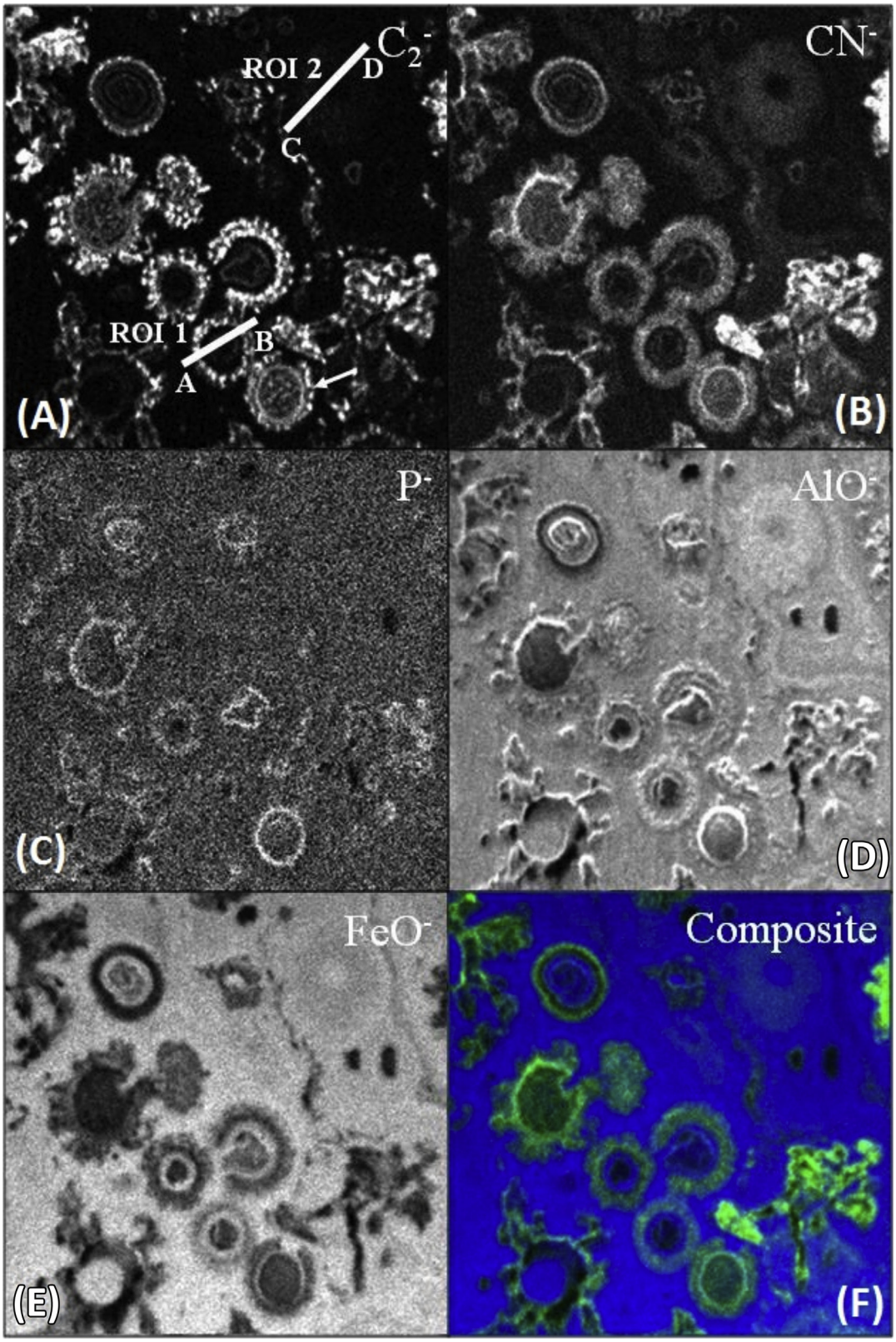

Figure 8. (A, B) NanoSIMS analysis of mineral encrusted cell envelopes are displayed as black and white intensity maps, with higher concentrations represented by white areas and lower concentrations displayed as darker regions. NanoSIMS micrographs highlight the preservation of carbon and nitrogen biosignatures associated with the microbial cell envelope. (C) Phosphorus was distributed throughout the sample and only enhanced due to edge effects associated with the hollow encrusted cell envelopes. (D, E) Aluminium and iron are present throughout the sample but aluminium appears to be slightly enriched where preserved organic biosignatures are preserved (refer to Fig. 9). In contrast, iron concentrations are reduced in regions where organic carbon and nitrogen are preserved. (F) The composite micrographs highlights the poor correlation of iron (blue) with preserved organic nitrogen (green). All micrographs are 8 μm × 8 μm.

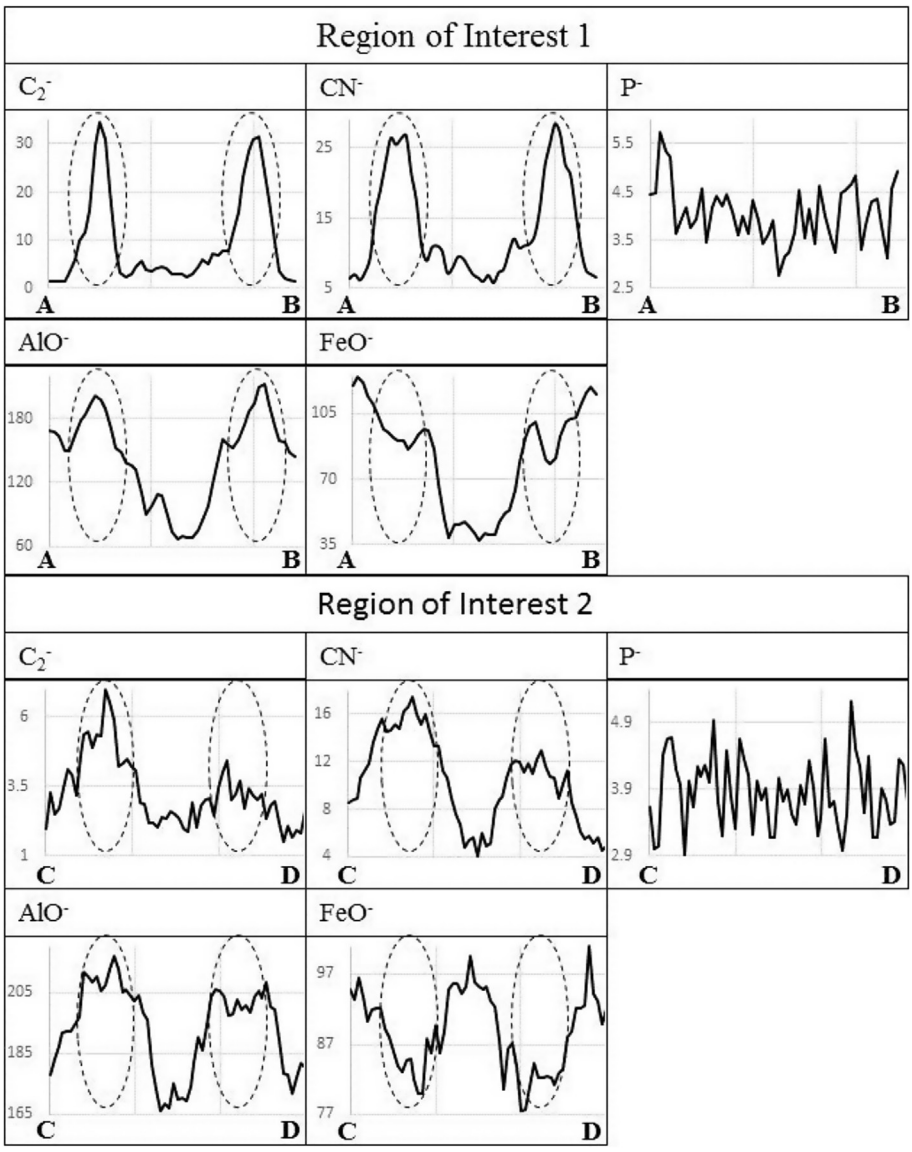

Figure 9. Intensity line plots of ion counts plotted against pixel distance cross-cutting microfossils for a partially infilled microfossil (Fig. 8; ROI 1) and a completely infilled microfossil (Fig. 8; ROI 2). For ROI 1, aluminium is enhanced in association with the organic biosignatures and was slightly enriched in regions where organic carbon and nitrogen are preserved. Iron poorly correlates with organic carbon and nitrogen and is slightly increased in intracellular lumen. Similarly, for the completely infilled cell (Fig. 8; ROI 2), aluminium is enhanced in regions with the preserved organic carbon and nitrogen. Note, iron is out of phase with the preserved organic biosignatures. Phosphorus is relatively consistent for both ROI 1 and 2, highlighting these cells were not affected by edge enhancements.

(biofilms) are present throughout the ferruginous duricrust sample (Fig. 2). Microfossils within the lake-edge sample had putatively grown within the lake environment (pH 5.6–5.8).

Permineralised microfossils were analysed for the preservation of chemical biosignatures using NanoSIMS in the location highlighted in Fig. 3. NanoSIMS analysis highlights that aluminium and phosphorus are enriched around all permineralised microfossils, with phosphorus distribution showing an affinity with aluminium (Fig. 4; $r = 0.41$). Phosphorus enrichment around permineralised microfossils cannot be considered an organic biosignature: it is simply a consequence of the preferential sorbtion of phosphorus to aluminium-substituted iron oxide minerals (Schulze and Schwertmann, 1984; Ruan and Gilkes, 1996). In contrast, iron is enriched within the intracellular regions of microbial fossils. Carbon and nitrogen biosignatures are also not preserved in association with permineralised microfossils (Fig. 4). In the absence of organic biosignatures associated with permineralised microfossils, the enrichment of aluminium around permineralised microfossils is responsible for the structural preservation of the microorganisms. The structural preservation of microfossils indicates that the iron-aluminium oxide minerals had not undergone a significant alteration or dissolution event.

3.2. Encrusted cell envelopes

The pH of the goethite-cemented vein cross-cutting the saprolite in which the encrusted cell envelopes were identified was approximately 6.3. The primary mineralogy of goethite and hematite (Supplementary Fig. A2) is supported by the high iron content (57.9 wt.%). Relatively low bulk-rock Al_2O_3 (2.54 wt.%) and SiO_2 (1.55 wt.%) concentrations are present with minor TiO_2 (0.2 wt.%) and P (0.24 wt.%) (Table 1). Encrusted microbial cell envelopes are preserved throughout the goethite-rich vein that

Table 1
Bulk chemical and mineralogical characteristics and the primary fossilisation texture associated with the ferruginous duricrust sample and the goethite-cemented sample (all elements in wt.%).

Characterisation	Ferruginous duricrust	Goethite-cemented vein
pH	6.5	6.3
XRD: Bulk sample mineralogy	Goethite, hematite, kaolinite (Supplementary Fig. A1)	Goethite, hematite (Supplementary Fig. A2)
FTIR: Mineralogy associated with microbial fossils	Kaolinite (Levett et al., 2016)	Gibbsite (Supplementary Fig. A3)
Dominant fossilisation textures	Pemineralised microfossils (Figs. 3–5)	Encrusted cell envelopes (Figs. 2, 6–8)
Al_2O_3	8.63	2.54
As	0.005	0.005
Ba	<0.001	<0.001
CaO	0.01	0.01
Cl	0.004	0.003
Co	0.001	<0.001
Cr_2O_3	0.023	0.0004
Cu	0.003	<0.001
Fe	52.64	57.90
K_2O	0.001	<0.001
MgO	0.01	<0.01
Mn	0.027	0.008
Na_2O	0.020	0.005
Ni	<0.001	<0.001
P	0.227	0.240
Pb	<0.001	<0.001
S	0.056	0.027
SiO_2	4.92	1.55
Sn	<0.001	<0.001
Sr	<0.001	<0.001
TiO_2	0.85	0.2
V	0.081	<0.001
Zn	<0.001	<0.001
Zr	0.014	<0.001
LOI	9.32	12.10
Total	99.92	99,65

cross-cut the hematite-enriched saprolite in Serra do Gandarela, Quadrilátero Ferrífero (Fig. 5). In contrast to the pemineralised microfossils, SEM-EDS and FTIR microspectroscopy reveals that mineralised microbial cell envelopes are preserved within the pore spaces between with gibbsite clasts (Supplementary Figs. A3–A4). Secondary electron micrographs reveal that the three-dimensional (3D) structure of rod-shaped microfossils is preserved within pore spaces (Fig. 5B). Encrusted cell envelopes are typically rod-shaped and approximately 1 μm in diameter and 1.5 μm in length (Fig. 5B). Ferruginised plant roots could not be identified in thin samples using scanning electron microscopy, therefore the distribution of microfossils with respect to plant roots is not apparent.

A variety of fossilisation textures were associated with the encrusted cell envelopes (Fig. 7). The carbon and carbon-nitrogen NanoSIMS elemental micrographs highlight that cell envelope biosignatures associated with the mineralised cell envelopes are preserved (Fig. 8). The intracellular regions of fossilised cell envelopes are infilled with secondary iron oxide minerals to varying degrees, ranging from completely void (Fig. 8; white arrow), partially infilled (Fig. 8; Region of Interest (ROI) 1) and completely infilled microfossils (Fig. 8; ROI 2). The completely infilled microfossil shares a similar chemical signature with the pemineralised microfossils: iron-enriched intracellularly and aluminium enriched around the microfossil (Fig. 8). The carbon and nitrogen intensities are lower for the completely infilled microfossil compared with the partially infilled and void microfossils (Figs. 8 and 9).

Cross-sections of individual microfossils reveals that aluminium is enhanced in regions with preserved carbon and nitrogen (organic) biosignatures (Fig. 9). A cross-section of a partially infilled microbial fossil (Fig. 8; ROI 1) highlights that aluminium is enhanced with the preserved cell envelope structures and correlates well with preserved carbon ($r = 0.67$) and nitrogen ($r = 0.76$; Fig. 9). In contrast, the relative iron concentration is depleted in locations and poorly correlates with preserved carbon ($r = 0.13$) and nitrogen ($r = 0.24$) biosignatures. The relative iron concentration appears to be reduced for all microfossils in regions where carbon and nitrogen biosignatures are preserved (Fig. 8). Similarly, a cross-section of the completely infilled cell (ROI 2) reveals that aluminium is slightly enriched in regions where organic biosignatures are preserved (Fig. 9). Aluminium positively correlates with the preserved carbon ($r = 0.76$) and nitrogen ($r = 0.88$) biosignatures (Fig. 9) in the completely infilled microfossil (Fig. 8). In comparison, iron negatively correlates with preserved organic biosignatures and aluminium (Fig. 9).

4. Discussion

The microfossils in the present study are all preserved within iron-rich rocks, with a bulk iron concentration of approximately 52.64% for the ferruginous duricrust (permineralised microfossils) sample and 57.90% for the goethite-cemented vein (encrusted cell envelopes). Iron biomineralisation has been suggested to represent the first stages of microbial fossilisation and may be essential for the structural integrity of cell components after cell death (Ferris et al., 1988; Miot et al., 2009a, b; Schädler et al., 2009; Miot et al., 2011; Li et al., 2013, 2014; Picard et al., 2015). Therefore, iron was hypothesised to drive the fossilisation of the microfossils presented here. The reduced iron concentration and the enrichment of aluminium associated with preserved organic biosignatures (Figs. 8 and 9) suggests that aluminium complexing with cell envelope structures before or immediately after cell death may have been responsible for the preservation of organic biosignatures associated with encrusted cell envelopes. Aluminium complexation with organic cell envelopes appears to resist autolytic degradation of cell envelope structures following cell death and contributes to the preservation of organic biosignatures associated with encrusted microfossils (Figs. 8 and 9).

Carbon and nitrogen biosignatures were not preserved with the permineralised microfossils. In the absence of preserved organic biosignatures, aluminium enrichment around permineralised microfossils was responsible for the structural preservation of the permineralised microfossils within iron-rich duricrusts (Figs. 2–4). The NanoSIMS micrographs presented here indicate that aluminium may play a critical role in the structural and physicochemical preservation of microfossils within iron-rich environments.

Iron-aluminosilicate minerals have been demonstrated to mineralise cell envelope structures of microorganisms (Ferris et al., 1987). To date, research has focused on the role of iron in microbial fossilisation and biosignature preservation (Ferris et al., 1988; Miot et al., 2011; Li et al., 2013; Picard et al., 2015). Iron-organic complexes have been proposed to represent the initial stages of microbial fossilisation in iron-rich environments (Li et al., 2013), resisting the degradation of organic biosignatures (Picard et al., 2015). The data presented here indicate that aluminium ions binding with microbial cell envelope structures may increase the successful fossilisation and the preservation of organic biosignatures within the geologic record.

The iron-rich duricrust sample and the goethite cemented vein both had a circumneutral pH, therefore aluminium should be relatively immobile within these environments (Bache, 1986). Within the duricrust sample, permineralised microfossils (Fig. 2) were routinely identified within proximity to highly weathered kaolinite-rich clasts that may have been actively weathered by microorganisms via the exudation of organic acids. The encrusted microbial cell envelopes (Fig. 5) were identified in the pore space between gibbsite grains within the goethite-cemented vein. Given the stability of gibbsite in circumneutral environments, the production of organic acids is likely to control the release of aluminium from gibbsite clasts (Bache, 1986). Weathering of gibbsite grains (Fig. 1) may have released aluminium ions into solution, contributing to microbial fossilisation and preservation. Aluminium and phosphorus can be present in unweathered BIFs in Brazil (Dorr, 1973), which can be enriched and maintained within the ferruginous duricrusts and the saprolite of highly weathered BIFS (Dorr, 1964).

4.1. Permineralised microfossils

In the absence of chemical biosignatures associated with the permineralised microfossils, bacteriomorphic structures were determined to represent remnant microorganisms using the guide by Westall (1999). The biogenicity of permineralised microfossils was determined based on cell size (1–2 μm in length), shape (rod-shaped with curved ends), evidence for cell replication (Fig. 3) and microbial colony formation (Fig. 2). Permineralised microbial biofilms within ferruginous duricrusts have previous been demonstrated to colonise in proximity to and along the grain boundaries of kaolinite-rich clasts (Levett et al., 2016). The preservation of subcellular structures including periplasmic structures may be preserved associated with microfossils despite the pseudomophic mineral replacement of the majority of organic carbon associated with the initial microbial cell (Cosmidis et al., 2013). High resolution micrographs of permineralised microfossils identified in iron-rich duricrusts that highlights the preservation of rod-shaped microfossils with evidence of binary fission, cell envelope bilayers and filamentous bacteriomorphs have previously been published (Levett et al., 2016). NanoSIMS analysis of permineralised microfossils identified within an iron-rich duricrust that capped iron ore deposits demonstrates that aluminium was critical to the structural preservation of microfossils. All permineralised microfossils shared a consistent fossilisation chemical signature: aluminium enriched around the microfossils and iron enriched within the remnant cell. Organic biosignatures are not preserved in association with the permineralised microfossils, possibly replaced by the pseudomorphic precipitation of iron and aluminium oxide minerals that have structurally preserved the microfossils (Cosmidis et al., 2013).

4.2. Encrusted cell envelopes

The preservation of organic carbon and nitrogen associated with the encrusted cell envelope fossils (Fig. 8) agrees with the 3D preservation of rod-shaped microfossils (Fig. 5B). Cosmidis et al. (2013) observed similar fossilisation textures within a coprolite, with calcium phosphate minerals forming around microfossils and infilling remnant cells to varying extents. NanoSIMS analysis of encrusted cell envelopes highlights that aluminium is enhanced in association with preserved carbon and nitrogen and may play a direct role in the preservation of organic biosignatures associated with the microbial cell envelopes.

Aluminium has previously been demonstrated to bind to cell envelope structures in *E. coli*, inhibiting cell growth (Guida et al., 1991) but the role that aluminium may play in microbial fossilisation and the preservation of organic biosignatures has not, to the best of the authors knowledge, previously been reported. Preserved carbon and nitrogen biosignatures associated with microfossils must have resisted enzymatic and oxidative degradation despite being fossilised within a highly oxidising environment, evidenced from the primary iron oxide minerals being goethite and hematite. Iron was relatively depleted in locations where carbon and nitrogen biosignatures are preserved (Fig. 8); however, iron oxide precipitates have contributed to cell envelope preservation by extending the mineral encrustation around the microfossils. The additional mineralisation of cell envelopes is likely to have reduced the exposure of carbon and nitrogen biosignatures to chemical and enzymatic degradation. These results indicate the resistance of aluminium to changes in oxidation potential may promote the preservation of organic biosignatures (Bache, 1986).

Encrusted cell envelopes with differing degrees of secondary iron oxide infilling and organic biosignature preservation allows for the investigation of microfossil weathering. In the present study, internal mineral precipitates nucleated at the membrane-cytoplasm boundary, forming a continuous layer parallel with cell membrane (Fig. 8; ROI 1). Secondary mineral growth may then continue from the membrane-cytoplasm boundary and infill the cytoplasm of remnant cells. These observations are consistent with laboratory (Benzerara et al., 2004) and environmental studies (Cosmidis et al., 2013) investigating internal mineral precipitates. Analysis of the partially infilled microbial fossil (Fig. 8; ROI 1) highlights that aluminium concentrations continue to decrease in intracellular regions where no organic carbon or nitrogen is preserved. In contrast, iron concentrations are slightly increased in intracellular regions (Fig. 9). For the completely infilled cell (Fig. 8: ROI 2), carbon and nitrogen associated with the cell envelope were reduced, indicating that it may represent a more advanced stage of environmental weathering and recrystallisation compared with partially infilled encrusted cell envelopes. The completely infilled cells shared a similar chemical signature with the permineralised microfossils: iron enriched within intracellular regions and aluminium-enriched around the microfossil.

The preservation of organic biosignatures associated with microorganisms are typically investigated by increasing temperature and pressure to simulate diagenesis (Oehler and Schopf, 1971; Beveridge et al., 1983; Li et al., 2014; Picard et al., 2015). The reduced carbon and nitrogen signal in the completely infilled cell (Fig. 8; ROI 2) indicates that the continuous precipitation of minerals during weathering, not exposure to increased temperatures and pressures, may be a limiting factor for the preservation of

organic biosignatures. Therefore, low temperature and pressure weathering experiments are required to assess the preservation of organic biosignatures associated with microfossils in iron-rich environments.

4.3. A model for the role of aluminium in microbial fossilisation

In agreement with the fossilisation textures presented here, Londono et al. (2017) demonstrated aluminium colocalised with cell envelope structures (in comparison with intracellular regions), while iron concentrations were enriched within intracellular regions. Aluminium complexation with phosphate groups of plasma membranes has been demonstrated to destabilise the membrane structures and disrupt the membrane permeability (Deleers et al., 1985, 1986), which may allow iron to permeate into the intracellular regions and restricting intracellular aluminium transportation (Londono et al., 2017).

The intensity cross-section of the completely infilled microbial fossil (Fig. 8; ROI 2) displays a similar elemental distribution to the permineralised microfossils (Figs. 2–4): aluminium enriched around the cell envelope and iron enriched within the intracellular regions of the microfossil. Microbial plasma membrane structures that resist the transportation of aluminium ions into intracellular regions (Londono et al., 2017) may have resulted in the nucleation of aluminium-enriched minerals on microbial cell surfaces. Aluminium may then be further enriched by the preferential inclusion of aluminium into these aluminium-enriched minerals. The pseuomorphic precipitation of iron and aluminium minerals from solution is likely to replace the organic biosignatures. The permineralised microfossils may represent a more advanced stage of microfossil weathering compared with the encrusted cell envelopes that showed a similar chemical signature when completely infilled (Fig. 8; ROI 2).

The enrichment of aluminium around preserved microfossils and the enrichment of iron within intracellular regions requires explanation. Trivalent iron and aluminium are known to have a strong affinity for anions capable of donating oxygen. Inorganic and organic phosphates therefore present ideal ligands for aluminium and iron complexation. Membrane phosphate end groups have been proposed to have the following preferential affinity for iron and aluminium cations: $Fe^{3+} > Al^{3+} > Fe^{2+}$ (Zatta et al., 2002). Therefore, the poor Fe correlation with preserved organic biosignatures presented here is unexpected and is likely to be explained by aluminium forming an effectively irreversible complex with extracellular organic substances. Aluminium has been demonstrated to bind tenaciously with Mg-dependent enzymes, with exchange rates of approximately 10^5 slower than Mg. The formation of enzymatically unavailable aluminium-organic complexes may contribute to resisting the degradation of organic biosignatures (Ferris et al., 1988). Additional work is required to demonstrate the preservation of aluminium-organic complexes associated with mineral encrusted microbial cell envelopes.

4.4. The relative age of microfossils

Geochronological data has demonstrated that the ferruginous duricrusts that cap BIFs in Brazil tend to increase in age with depth (Shuster et al., 2012; Monteiro et al., 2014). The top 10 m of the ferruginous duricrust from the Carajás (N4C) mineral province has an approximate average age of 8.25 Ma and samples from the top 2 cm of the profile have an approximate age of 0.9 Ma (Shuster et al., 2012). The ferruginous duricrust sample containing permineralized microfossils was collected directly from the surface (Levett et al., 2016). Therefore, the permineralised microfossils presented here are likely to date to less than 0.9 Ma. Biological mechanisms have been postulated to drive the biogeochemical cycling of iron within the ferruginous duricrusts that cap BIFs (Monteiro et al., 2014). Microfossils in the uppermost crust are therefore likely to have experienced an increased exposure to iron-rich solutions, mineral precipitation and weathering, which appears to have replaced organic biosignatures.

Within a single profile, the saprolite has been demonstrated to have mineralised prior to the overlying ferruginous duricrust (Monteiro et al., 2014). Goethite grains from the saprolite of the Gandarela Syncline have produced dates of approximately 2–55 Ma (Monteiro et al., 2014). Therefore, the encrusted cell envelopes identified within the vein that cross-cut the saprolite are likely to have a greater age than the permineralised microfossils identified in the ferruginous duricrust.

5. Conclusions

High resolution NanoSIMS maps of permineralised microfossils and mineral encrusted microbial cell envelopes identified in iron-rich rocks indicates that aluminium may play an important role in the structural and physiochemical preservation of microbial fossils. In the absence of preserved organic biosignatures, aluminium enrichment around permineralised microfossils governs the structural preservation of microorganisms within an iron-rich duricrust that caps iron ore deposits in Brazil. The pseudomorphic precipitation of aluminium and iron oxide minerals associated with permineralised microfossils appears to replace the preservation of organic biosignatures associated with microfossils in iron-rich rocks. For mineralised cell envelope structures, aluminium is enhanced in regions with preserved organic carbon and nitrogen, indicating that aluminium complexation with microbial cell envelopes inhibits the enzymatic and oxidative degradation of organic biosignatures.

Acknowledgements

We acknowledge support from the Vale S.A.-UQ Geomicrobiology initiative and the Australian Research Council Linkage Program (LP140100805) to G. Southam and P. Vasconcelos. The authors acknowledge the facilities and the scientific and technical assistance of the Australian Microscopy and Microanalysis Research Facility at the Centre of Microscopy and Microanalysis, at the University of Queensland. Alan Levett acknowledges the support from the Australian Government Research Training Program.

Appendix A. Supplementary data

Supplementary data related to this article can be found at https://doi.org/10.1016/j.gsf.2018.06.006.

References

Bache, B.W., 1986. Aluminium mobilization in soils and waters. Journal of the Geological Society 143, 699.

Benzerara, K., Menguy, N., Guyot, F., Skouri, F., de Luca, G., Barakat, M., Heulin, T., 2004. Biologically controlled precipitation of calcium phosphate by *Ramlibacter tataouinensis*. Earth and Planetary Science Letters 228, 439–449.

Beveridge, T., Meloche, J., Fyfe, W., Murray, R., 1983. Diagenesis of metals chemically complexed to bacteria: laboratory formation of metal phosphates, sulfides, and organic condensates in artificial sediments. Applied and Environmental Microbiology 45, 1094–1108.

Brasier, M.D., Antcliffe, J., Saunders, M., Wacey, D., 2015. Changing the picture of Earth's earliest fossils (3.5–1.9 Ga) with new approaches and new discoveries. Proceedings of the National Academy of Sciences 112, 4859–4864.

Cosmidis, J., Benzerara, K., Gheerbrant, E., Estève, I., Bouya, B., Amaghzaz, M., 2013. Nanometer-scale characterization of exceptionally preserved bacterial fossils in Paleocene phosphorites from Ouled Abdoun (Morocco). Geobiology 11, 139–153.

Deleers, M., Servais, J.-P., Wülfert, E., 1985. Micromolar concentrations of Al^{3+} induce phase separation, aggregation and dye release in phosphatidylserine-containing lipid vesicles. Biochimica et Biophysica Acta (BBA) - Biomembranes 813, 195–200.

Deleers, M., Servais, J.-P., Wülfert, E., 1986. Neurotoxic cations induce membrane rigidification and membrane fusion at micromolar concentrations. Biochimica et Biophysica Acta (BBA) - Biomembranes 855, 271–276.

Dorr, J.V.N., 1964. Supergene iron ores of Minas Gerais, Brazil. Economic Geology 59, 1203–1240.

Dorr, J.V.N., 1973. Iron-formation in south America. Economic Geology 68, 1005–1022.

Exley, C., Birchall, D., 1992. The cellular toxicity of aluminium. Journal of Theoretical Biology 159, 83–98.

Ferris, F.G., Fyfe, W.S., Beveridge, T.J., 1987. Bacteria as nucleation sites for authigenic minerals in a metal-contaminated lake sediment. Chemical Geology 63, 225–232.

Ferris, F.G., Fyfe, W.S., Beveridge, T.J., 1988. Metallic ion binding by *Bacillus subtilis*: implications for the fossilization of microorganisms. Geology 16, 149–152.

Guida, L., Saidi, Z., Hughes, M.N., Poole, R.K., 1991. Aluminium toxicity and binding to *Escherichia coli*. Archives of Microbiology 156, 507–512.

Heaney, P.J., Vicenzi, E.P., Giannuzzi, L.A., Livi, K.J., 2001. Focused ion beam milling: a method of site-specific sample extraction for microanalysis of Earth and planetary materials. American Mineralogist 86, 1094–1099.

Hoppe, P., Cohen, S., Meibom, A., 2013. NanoSIMS: technical aspects and applications in cosmochemistry and biological geochemistry. Geostandards and Geoanalytical Research 37, 111–154.

Jacobi, C.M., Carmo, F.F., 2011. Life-forms, pollination and seed dispersal syndromes in plant communities on ironstone outcrops, SE Brazil. Acta Botanica Brasilica 25, 395–412.

Konhauser, K.O., Jones, B., Phoenix, V.R., Ferris, G., Renaut, R.W., 2004. The microbial role in hot spring silicification. AMBIO: A Journal of the Human Environment 33, 552–558.

Levett, A., Gagen, E., Shuster, J., Rintoul, L., Tobin, M., Vongsvivut, J., Bambery, K., Vasconcelos, P., Southam, G., 2016. Evidence of biogeochemical processes in iron duricrust formation. Journal of South American Earth Sciences 71, 131–142.

Li, J., Benzerara, K., Bernard, S., Beyssac, O., 2013. The link between biomineralization and fossilization of bacteria: insights from field and experimental studies. Chemical Geology 359, 49–69.

Li, J., Bernard, S., Benzerara, K., Beyssac, O., Allard, T., Cosmidis, J., Moussou, J., 2014. Impact of biomineralization on the preservation of microorganisms during fossilization: an experimental perspective. Earth and Planetary Science Letters 400, 113–122.

Londono, S.C., Hartnett, H.E., Williams, L.B., 2017. Antibacterial activity of aluminum in clay from the Colombian Amazon. Environmental Science & Technology 51, 2401–2408.

Macdonald, T.L., Martin, B.R., 1988. Aluminum ion in biological systems. Trends in Biochemical Sciences 13, 15–19.

Marshall, C.P., Emry, J.R., Marshall, A.O., 2011. Haematite pseudomicrofossils present in the 3.5-billion-year-old apex chert. Nature Geoscience 4, 240.

Martin, R.B., 1986. The chemistry of aluminum as related to biology and medicine. Clinical Chemistry 32, 1797.

Miot, J., Benzerara, K., Morin, G., Kappler, A., Bernard, S., Obst, M., Férard, C., Skouri-Panet, F., Guigner, J.-M., Posth, N., Galvez, M., Brown Jr., G.E., Guyot, F., 2009a. Iron biomineralization by anaerobic neutrophilic iron-oxidizing bacteria. Geochimica et Cosmochimica Acta 73, 696–711.

Miot, J., Benzerara, K., Obst, M., Kappler, A., Hegler, F., Schädler, S., Bouchez, C., Guyot, F., Morin, G., 2009b. Extracellular iron biomineralization by photoautotrophic iron-oxidizing bacteria. Applied and Environmental Microbiology 75, 5586–5591.

Miot, J., Maclellan, K., Benzerara, K., Boisset, N., 2011. Preservation of protein globules and peptidoglycan in the mineralized cell wall of nitrate-reducing, iron (II)-oxidizing bacteria: a cryo-electron microscopy study. Geobiology 9, 459–470.

Monteiro, H.S., Vasconcelos, P.M., Farley, K.A., Spier, C.A., Mello, C.L., 2014. (U–Th)/He geochronology of goethite and the origin and evolution of cangas. Geochimica et Cosmochimica Acta 131, 267–289.

Oehler, J.H., Schopf, J.W., 1971. Artificial microfossils: experimental studies of permineralization of blue-green algae in silica. Science 174, 1229–1231.

Picard, A., Kappler, A., Schmid, G., Quaroni, L., Obst, M., 2015. Experimental diagenesis of organo-mineral structures formed by microaerophilic Fe(II)-oxidizing bacteria. Nature Communications 6.

Preston, L., Shuster, J., Fernández-Remolar, D., Banerjee, N., Osinski, G., Southam, G., 2011. The preservation and degradation of filamentous bacteria and biomolecules within iron oxide deposits at Rio Tinto, Spain. Geobiology 9, 233–249.

Riding, R., 2000. Microbial carbonates: the geological record of calcified bacterial–algal mats and biofilms. Sedimentology 47, 179–214.

Ruan, H.D., Gilkes, R.J., 1996. Kinetics of phosphate sorption and desorption by synthetic aluminous goethite before and after thermal transformation to hematite. Clay Minerals 63.

Salama, W., El Aref, M., Gaupp, R., 2013. Mineral evolution and processes of ferruginous microbialite accretion—an example from the Middle Eocene stromatolitic and ooidal ironstones of the Bahariya Depression, Western Desert, Egypt. Geobiology 11, 15–28.

Schädler, S., Burkhardt, C., Hegler, F., Straub, K., Miot, J., Benzerara, K., Kappler, A., 2009. Formation of cell-iron-mineral aggregates by phototrophic and nitrate-reducing anaerobic Fe (II)-oxidizing bacteria. Geomicrobiology Journal 26, 93–103.

Schulze, D.G., Schwertmann, U., 1984. The influence of aluminium on iron oxides; X, Properties of Al-substituted goethites. Clay Minerals 19, 521–539.

Shuster, D.L., Farley, K.A., Vasconcelos, P.M., Balco, G., Monteiro, H.S., Waltenberg, K., Stone, J.O., 2012. Cosmogenic ^{3}He in hematite and goethite from Brazilian "canga" duricrust demonstrates the extreme stability of these surfaces. Earth and Planetary Science Letters 329, 41–50.

Spier, C., de Oliveira, S., Rosière, C., 2003. Geology and geochemistry of the águas claras and pico iron mines, quadrilátero ferrífero, Minas Gerais, Brazil. Mineralium Deposita 38, 751–774.

Westall, F., 1999. The nature of fossil bacteria: a guide to the search for extraterrestrial life. Journal of Geophysical Research: Planets 104, 16437–16451.

Zatta, P., Kiss, T., Suwalsky, M., Berthon, G., 2002. Aluminium(III) as a promoter of cellular oxidation. Coordination Chemistry Reviews 228, 271–284.